Taylor & Francis
Taylor & Francis Group

Integrated Ferroelectrics

An International Journal

ISSN: (Print) (Online) Journal homepage: https://www.tandfonline.com/loi/ginf20

Synthesis of Lithium Silicon Vanadium Oxide by Solid-State Reaction with Microwave-Assisted Method and Electrochemical Characterization

Jaturon Kumchompoo, Nattapol Laorodphan, Pinit Kidkhunthod, Phetlada Kunthadee & Ratchadaporn Puntharod

To cite this article: Jaturon Kumchompoo, Nattapol Laorodphan, Pinit Kidkhunthod, Phetlada Kunthadee & Ratchadaporn Puntharod (2022) Synthesis of Lithium Silicon Vanadium Oxide by Solid-State Reaction with Microwave-Assisted Method and Electrochemical Characterization, Integrated Ferroelectrics, 225:1, 1-11, DOI: 10.1080/10584587.2022.2054050

To link to this article: https://doi.org/10.1080/10584587.2022.2054050

Published online: 13 May 2022.

INTEGRATED FERROELECTRICS
2022, VOL. 225, 1–11
https://doi.org/10.1080/10584587.2022.2054050

Taylor & Francis
Taylor & Francis Group

Synthesis of Lithium Silicon Vanadium Oxide by Solid-State Reaction with Microwave-Assisted Method and Electrochemical Characterization

Jaturon Kumchompoo[a], Nattapol Laorodphan[a,b], Pinit Kidkhunthod[c], Phetlada Kunthadee[a], and Ratchadaporn Puntharod[a]

[a]Faculty of Science, Program in Applied Chemistry, Maejo University, Thailand; [b]Faculty of Science, Program in Industrial Chemistry and Textile Technology, Maejo University, Thailand; [c]Synchrotron Light Research Institute (Public Organization), Nakhon Ratchasima, Thailand

ABSTRACT

In this research, the synthesis of lithium silicon vanadium pentaoxide compounds is performed by the solid-state reaction and heated by a microwave. This combines the advantages of a solid-state reaction and the microwave method. The precursors were lithium nitrate, vanadium pentaoxide, and silica from rice husk ash. The conditions were studied according to grinding time and microwave heating. Each condition was examined for electrochemical properties by cyclic voltammetry. The grinding time at 6 hr and heating at 600 W for 5 min provided the highest specific capacitance of 376 F g^{-1}. The product morphology was determined to be irregular in shape by scanning electron microscopy. The X-ray diffraction and transmission electron microscopy results identify that the product was $Li_{3.6}Si_{0.6}V_{0.4}O_4$. X-ray absorption near edge structure technique found the oxidation of vanadium was V^{4+} and V^{5+}. Fourier transform infrared spectroscopy and resonance Raman spectroscopy exhibited the bonds of Si – O, Li – O, V – O – V, V = O and Si – O–Si.

ARTICLE HISTORY
Received 24 March 2021
Accepted 21 July 2021

KEYWORDS
Microwave-assisted; solid-state reaction; lithium vanadium silicon oxide; supercapacitors

Introduction

Solid-state reaction with the microwave assisted method is a fast and ecofriendly reaction which also reduces the effect of solvents during the reaction. This combines the advantages of a solid-state reaction and the microwave method. The solid-state reaction with the microwave assisted method is developed to prepare cathode materials and supercapacitors. The principle of the solid-state reaction with microwave assisted method is that reactants can produce heat through the absorption of electromagnetic energy. The microwave has strong penetration ability and the surface and the object can be heated simultaneously [1]. The microwave solid-state method is popular with inorganic synthesis involving the metal alloying process [2], metallic materials [3], metal-organic frameworks (MOFs) [4], and graphene-based materials [5]. Some metal powders or bulk metals (e.g. Fe, Co, V, Zn, Sn, Na, and K) are good microwave susceptors and heat up rapidly [6]. Since microwave offers rapid volumetric and penetrated heating, high reaction rates and selectivity, chemical synthesis by microwave solid-state synthesis is very efficient and energy saving. Thus, the

CONTACT Ratchadaporn Puntharod ratchadaporn_p@mju.ac.th

materials can be synthesized more quickly by the microwave solid state method than the conventional solid-state synthesis method. In regards to the sites of three Li^+ ions in the unit cell of the material, this rapid crystal growth can lead to a dramatic deviation between microwave solid-state and conventional solid-state synthesis methods [7].

Supercapacitors, a system for electrochemical energy storage and conversion, has attracted numerous interests because of its rapid charge and discharge rates, high power density, long cycle lifetime, and high reliability compared to conventional batteries [8]. The exploration of suitable electrode materials is the key challenge for the application of supercapacitors. Electrical-energy-storage devices with high power density and long cycling life hold great promise for a broad spectrum of applications, such as hybrid electric vehicles and power tools [9]. To boost the specific capacitance of supercapacitors, the specific capacitor of the electrode materials must be as high as possible to promote electrical capacitance [10]. Supercapacitors can be sorted into electrochemical double layer capacitors and pseudo capacitors based on their charge storage mechanism [11]. The synthesis method is one of the main factors influencing the electrochemical performance of cathode materials. The solid state reaction with microwave assisted method will give the product a higher purity from reactions that are directly affected by microwave waves [2]. The microwave field gives rise to a current traveling in phase of materials with the field and causing resistive heating in the sample. Generally, this mechanism is the dominant effect in solid materials and is referred to as conduction heating. The materials can contribute some pseudo capacitance to the composite electrode, yet the electrochemical stability of the supercapacitor often becomes poor due to the inherent instability of doped species under the electrochemical conditions, which is not desirable in practical applications [12]. The $Li_{3.6}Si_{0.6}V_{0.4}O_4$ compound shows higher lithium ion conductivity than Li_2SiO_3 which has less conductivity than the main phase $Li_{3.6}Si_{0.6}V_{0.4}O_4$. The Li^+ vacancies which are current carriers in Li_2SiO_3 composition increase with formation of solid solution with Li_2SiO_3 [13]. Kitchen et al. found that Li_2SiO_3 has good electrical conductivity and can enhance the conductivity of the material [14]. Li_3VO_4 has been reported by Li et al. which found that it can be used as an electrode material but has low electrical conductivity when other phases were in the experiment. Silica has been widely used and employed to create high-performance or highly functional materials over the last few decades. The excellent electrical and dielectric properties of silica are extensively used in dynamic random access memory and field effect transistors. The highly porous silica contributes to good electron transfer, thus increasing electrical conductivity [15].

In this research, $LiNO_3$, V_2O_5, and SiO_2 from rice husk ash were the precursors to synthesize the capacitor materials by the solid-state reaction with microwave assisted method. The various techniques were the tools for characterization. Specific capacitance was measured by the cyclic voltammetry method.

2. Experiments

2.1. Materials preparation and Synthesis

2.1.1. Preparation of silica from rice husk ash

Rice husk ash was soaked in 0.5 M of hydrochloric acid for 30 min and filtered, washed with deionized water and subsequently dried at 100 °C. The dried rice husk ash was calcine at 900 °C for 9 hr and analyzed by X-ray fluorescence (SiO_2 95.34%).

2.1.2. Synthesis of material

The mixture of lithium nitrate monohydrate (8.87 g), vanadium pentaoxide (18.37 g), and silica (6.14 g) was 7:2:1 by mole ratio with excess lithium nitrate. The mixture was crushed and ground into powder using a mortar by manual operation. The parameters included varied grinding time for 4 and 6 hr and heating power at 400 and 600 W for 5 min in a microwave oven.

2.2. Characterization

Fourier transform infrared spectroscopy (Perkin Elmer Spectrum RXI) was measured with 4 cm^1 resolution, 16 scanning and recorded spectra from 4000 to 400 cm^{-1}. Resonance Raman spectroscopy (Jobin Yvon Horiba T64000) measurement was conducted using triple monochromator at 50× microscope with a 532 nm exciting laser source. Phase identification of the products was conveyed by X-ray diffraction (Rigaku mini flex II) with Cu Kα radiation.

Synchrotron X-ray absorption near edge structure spectroscopy (XANES) at the vanadium K-edge using transmission mode was conducted at the Synchrotron Light Research Institute (Public Organization) Beamline (BL5.2), Nakhon Ratchasima, Thailand. Cyclic voltammetry (CH instruments (CH 1230, USA) was used for all electrochemical measurements. Ag/AgCl electrode (3 M KCl) was used as a reference electrode with a scan rate of 5 to 60 mV s^{-1} and the applied potential was studied in the range of −0.4-0.5 volts.

Scanning electron microscopy (TESCAN, VEGA3) and transmission electron microscopy (JEOL JEM-2010) were performed on all powder samples to study the shape of the products.

2.3. Electrochemical Measurement

2.3.1. Preparation of the working electrode (WE)

Nickel foam substrate (1 × 2 cm) (initial weight recorded) was used as a working electrode (WE). Each material including 32 mg of active material, 4 mg of carbon black, and 4 mg of polyvinylidene difluoride (PVDF) were mixed and then added to 400 µL of N-methyl-2 pyrrolidone (NMP). After mixing, 70 µL of the prepared solution was dropped onto the nickel foam electrode surface and dried at 70 °C overnight. The prepared electrode was compressed at 10 MPa to smooth out the electrode surface. Finally, the weight of the obtained electrode was recorded. The difference between electrode weights before and after modification provided the weight of substance modified onto the electrode surface. Electrochemical properties were tested by cyclic voltammetry (CV).

2.3.2. Calculation of the specific capacitance

The specific capacitance (C) from the GCD technique by Yan et al. can be calculated with Equation (1) [16].

$$C = \frac{\int IdV}{\nu m V} \tag{1}$$

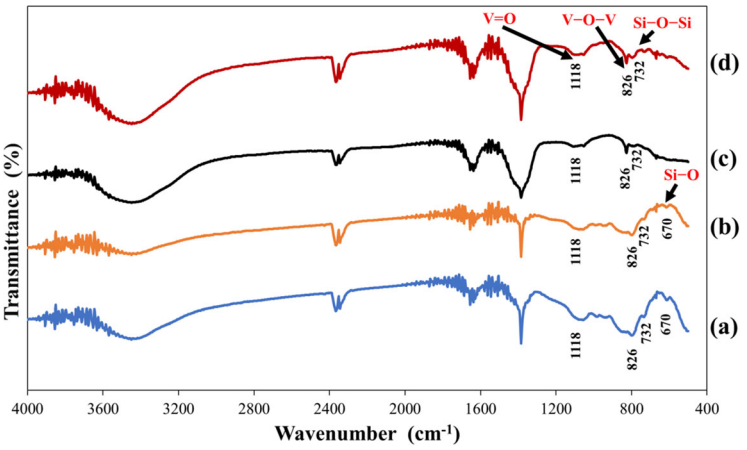

Figure 1. FTIR spectra of conditions (a) 4 hr-400W, (b) 4 hr-600W (c) 6 hr-400W and (d) 6 hr-600W.

where
C is the specific capacitance (F g^{-1})
I is the response current density (A cm^{-2})
V is the potential (V)
ν is the potential scan rate (mV s^{-1}),
and m is the mass of the electroactive materials in the electrodes (g),

3. Results and Discussion

3.1. Fourier Transform Infrared Spectroscopy (FTIR)

Figure 1 presents the FTIR spectra of products from lithium nitrate, vanadium pentaoxide, and silica from rice husk ash with a milling time of 4 and 6 hr, and heating by microwave at 400 and 600 W for 5 min. Interpreting the FTIR spectra results identifies the bands $\nu(Si-O)$ of SiO_2 at 670 cm^{-1} at the grinding time 4 hr, $\nu(Si-O-Si)$ at 732 cm^{-1} at 4 and 6 hr, and $(V-O-V)$ at 826 cm^{-1} $(V=O)$ bond at 1118 cm^{-1} [17, 19]. The band at 1384 cm^{-1} was assigned to nitrate [20].

3.2. Resonance Raman Spectroscopy (RR)

The RR spectra shown in Figure 2 indicate the Raman shift at 941 cm^{-1} assigned to the $(V=O)$ stretching was obtained as V_2O_5 precursor. When the microwave heating wattage increased, the intensity of the $(V=O)$ stretching peak increased gradually due to the higher crystallinity of 600 W products. In addition, the peaks at **8**77, 811, and 656 according to stretching of $\nu(Si-O)$ and 515 following to vibration of $\nu(Si-O-Si)$, vibration at 642 and 121 cm^{-1} were assigned to the vibrations of $\nu(Li-O)$ and 227 cm^{-1} can be assigned to the vibration of $\nu(V-O-V)$ [18, 19]. The Resonance Raman technique allows the vibrations of the $Li-O$ bond to occur in the product, which helps confirm that the product is lithium vanadium silicon oxide. Koroleva et al.

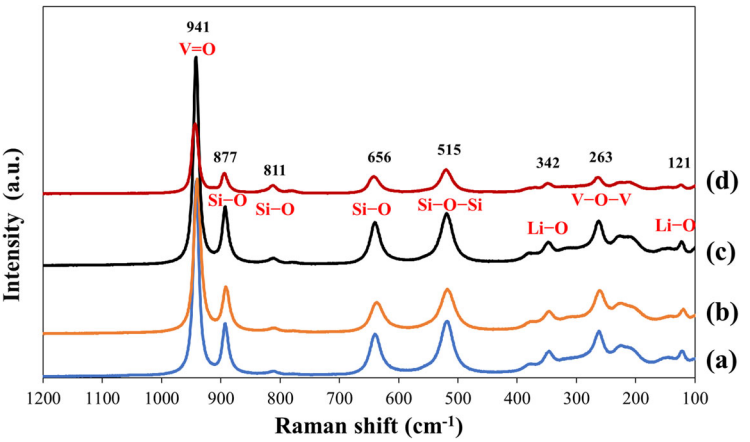

Figure 2. RR spectra of conditions (a) 4 hr-400W, (b) 4 hr-600W (c) 6 hr-400W and (d) 6 hr-600W.

(2007) found that when the synthesis temperature increases, the product mold of the silicate compound produced a significant increase in temperature [21].

3.3. X-Ray Diffraction (XRD)

The XRD results in Figure 3 show phase of product were mixed phase of $Li_{3.6}Si_{0.6}V_{0.4}O_4$, Li_3VO_4 and Li_2SiO_3. The higher crystallinity considering from sharp and higher intensity diffraction peaks were observed at the higher heating power (600 W) with the impurity of Li_2SiO_3. XRD pattern of product at 4 hr of griding time produced, an impurity phases were Li_3VO_4 and Li_2SiO_3, and the intensity of $Li_{3.6}Si_{0.6}V_{0.4}O_4$ was lower than 6 hr grinding time. The griding time for 6 hr found $Li_{3.6}Si_{0.6}V_{0.4}O_4$ with higher intensity peak and the impurity was only Li_2SiO_3. Hu et al. [22] reported Li_2SiO_3 could improve the electrochemical capability of oxide materials. Also, Quifen et al. [23] used Si-based material as Li_2SiO_3 to improve the electrical performances. On the other hand, the electrical conductivity of Li_3VO_4 is low ($<10^{-10}$ S m^{-1}) [24]. The performance was improved by Al insert into the structure of Li_3VO_4 [25]. It would be expected $Li_{3.6}Si_{0.6}V_{0.4}O_4$ contaminated with Li_2SiO_3 would show higher the specific capacitance than contaminated with Li_2SiO_3 and Li_3VO_4. Based on the XRD, the conditions at 6 hr of grinding time with both 400 and 600 W were further analyzed with other techniques due to the higher intensity than 4 hr of grinding time.

3.4. X-Ray Absorption near Edge Structure Analysis (XANES)

The XANES spectra in Figure 4 were compared with the V_2O_4 (V^{4+}) and V_2O_5 (V^{5+}) standard samples to identify the oxidation state of vanadium in all the samples. It is evident that their edge energies lie between V^{4+} and V^{5+}. The energy positions of the pre-edge, white line zone, and after absorption edge peaks in all samples match with the energy positions of the V_2O_3 and V_2O_5. For comparison, the XANES spectra in this work is similar to the results presented by Laorodphan *et al.* [26]. Moreover, the edge energies of all samples nearly overlap with the spectrum of V^{5+} standard, which implies that V in all samples exhibited a majority phase of V^{5+}. The whole of the spectra

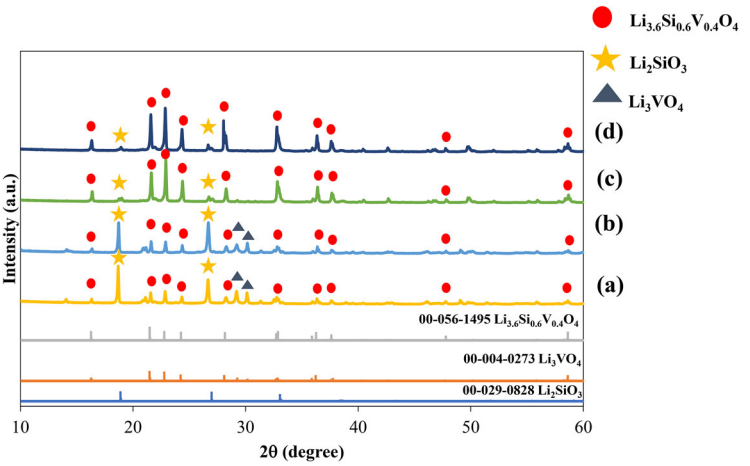

Figure 3. XRD patterns of the conditions(a) 4 hr-400W, (b) 4 hr-600W (c) 6 hr-400W and (d) 6 hr-600W.

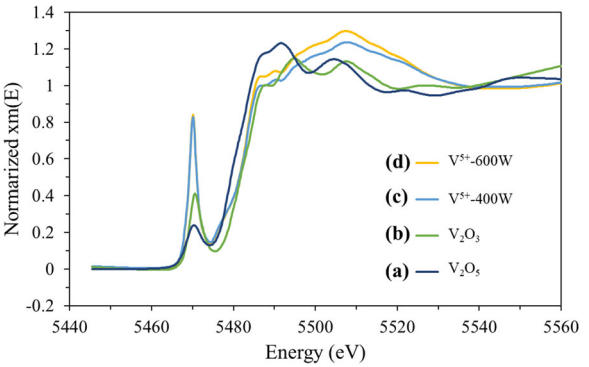

Figure 4. XANES spectra of conditions (a) V2O5 (b) V2O3 (c) 6 hr-400W and (d) 6 hr-600W.

showed an identified peak for vanadium edge and energy characteristic position of vanadium. The energy position of pre-edge peak is correlated with the charge of the vanadium ions. The high of pre-edge peak can also be useful for analyzing the local environment surrounding vanadium ions [27]. From the XANES spectra, vanadium with the oxidation number is V^{5+} corresponding to the phase found in XRD, which can help to confirm the formation compound of $Li_{3.6}Si_{0.6}V_{0.4}O_4$.

3.5. Electrochemical Measurement

Figure 5 shows the CV curves of the products at conditions 6 hr-400W and 6 hr-600W at different scan rates from 60 to 5 mV s^{-1} in 1 M KOH electrolyte solution. Each change profile shows a nearly flat region around 0.2-0.4 V. The redox profiles of V^{5+} correspond to the V^{4+}/V^{5+} redox couple at 0.25-0.38 V. XANES analysis indicates the mixed oxidation state of vanadium (V^{4+} and V^{5+}) of all products. The limitation of the cyclic voltammetry and Ag/AgCl reference electrode explain the V^{4+}/V^{5+} redox couple which is expected to be observed around 1.00 V [11, 22]. The calculated specific capacitance of the samples can be obtained from the integrated area of CV curve at a scan

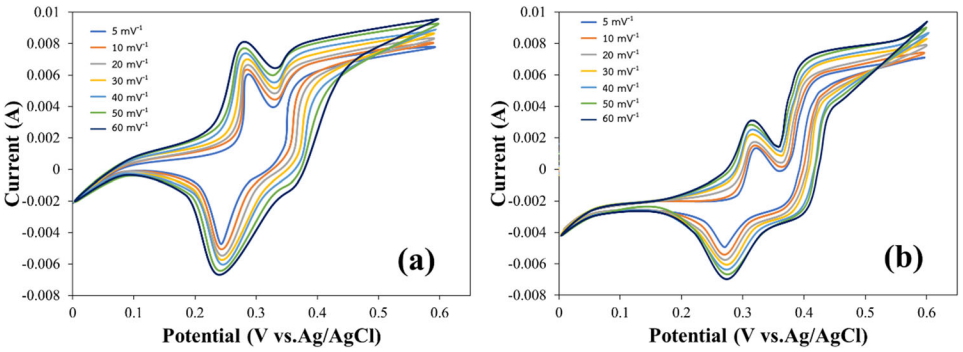

Figure 5. Cyclic voltammograms of conditions(a) 6 hr-400W and (b) 6 hr-600W.

rate of 60-5 mV s^{-1} using Equation (1). The calculated specific capacitance of all the electrodes at lower scan rates are significantly higher than those at higher scan rates, as depicted in Figure 6. The specific capacitance of condition 6 hr-400W and 6 hr-600W in range of 237-350 and 253-376 F g^{-1}, respectively. The 6 hr of grinding time and heating at 600 W provided the highest specific capacitance was 376 F g^{-1} at 5 mV s^{-1} of scan rate.

In Figure 6, the specific capacitance at 6 hr-600W was higher than 6 hr-400W as expected. Thus Li_2SiO_3 would enhance the specific capacitance of $Li_{3.6}Si_{0.6}V_{0.4}O_4$. The heating in a maximum magnetic-field of the standing wave can be efficient for samples with high electric conductivity. The high volumetric nature of microwave heating in silicon is relative with high conductivity [28]. Therefore, the condition at 600 W had higher conductivity than at 400 W.

3.6. Scanning Electron Microscopy (SEM)

Figure 7 presents the analysis using SEM techniques to analyze silica sources with Figure 7a and b at 400 W and (c and d) at 600 W of microwave heating. The products from the synthesis of silica from rice husk ash found that the crystalline products were clearly highly porous. This explains why products using silica from rice husk ash have a higher specific capacitance valence because of porous crystal [29]. There was an effect on the electron transfer in the reaction, causing the specific capacitance of different material. Considering the conductivity of silica, Bok et al. [30] found porous silica electrode synthesized with NaCl salts has high specific capacity. The microwave watt effect directly affects the porosity of the silica compound. The interaction of the electromagnetic wave from microwave oven with each molecule in solution at high heating can be influence during the hydrolysis-condensation process [31]. In the SEM image, 5000× magnification is evident that at 600 W microwave heating, the crystals have a significant increase in porousity. The increased porosity is the reason the synthesis at 600 W has a better specific capacitance than 400 W [32].

3.7. Transmission Electron Microscopy (TEM)

The bright field image in Figure 8 is the high magnification images that show the particles are porous in nature. Figure 8b, crystal was clear and thick layers which indicated the black solid part was very high content of vanadium and highly crystalline microstructure of $Li_{3.6}Si_{0.6}V_{0.4}O_4$ [33, 34]. The results of TEM-EDX will be used to calculate

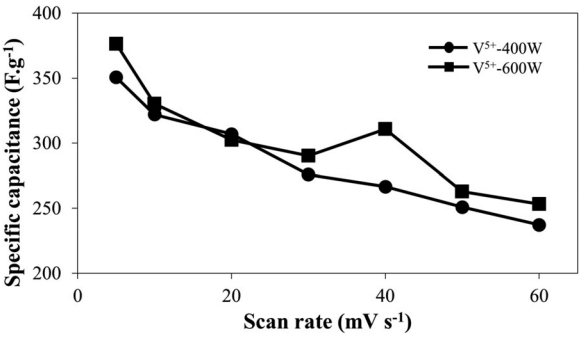

Figure 6. Plot of specific capacitance versus scan rate of 6 hr-400W and 6 hr-600W.

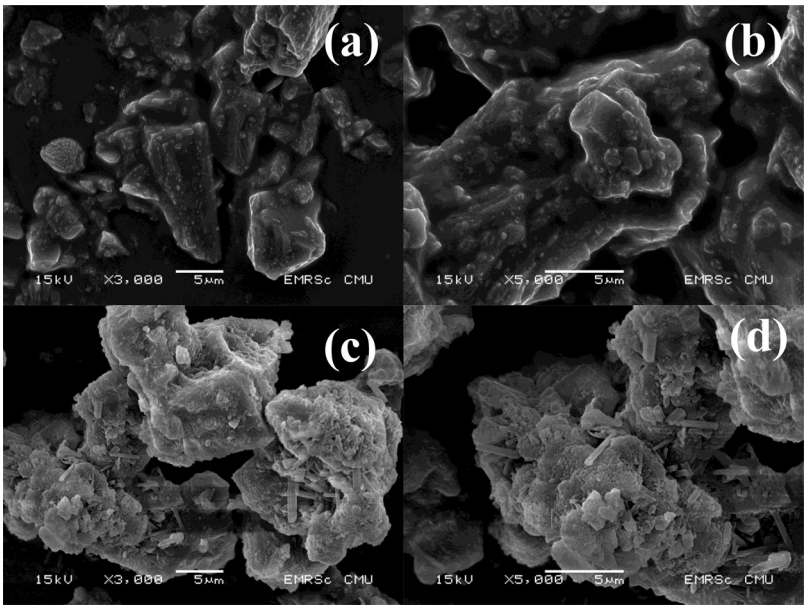

Figure 7. SEM images of (a) 6 hr-400W-3000× (b) 6 hr-400W-5000× (c) 6 hr-600W-3000× and (d) 6 hr-600W-5000×.

mole atoms from the percentage of atoms. In Figure 8a and c, the mole ratio of Si:V is 49:1. The high amount of Si is the remaining Si from the reactants during the synthesis and Li_2SiO_3 regarding to XRD results. This corresponds to the specific capacitance of synthesized product at 400 W has poor specific capacitance due to incomplete the formation of $Li_{3.6}Si_{0.6}V_{0.4}O_4$. In the Figure 8b and d, the mole ratio of Si:V is 1.3:1 similarly with the mole ratio of Si:V in $Li_{3.6}Si_{0.6}V_{0.4}O_4$. The mole ratio calculation from EDX corresponded with the specific capacitance at 600 W is higher than 400 W due to the completed forming of $Li_{3.6}Si_{0.6}V_{0.4}O_4$.

4. Conclusion

$Li_{3.6}Si_{0.6}V_{0.4}O_4$ was synthesized by solid-state reaction with the microwave-assisted method with rapid condition with shorter time than conventional solid state combined

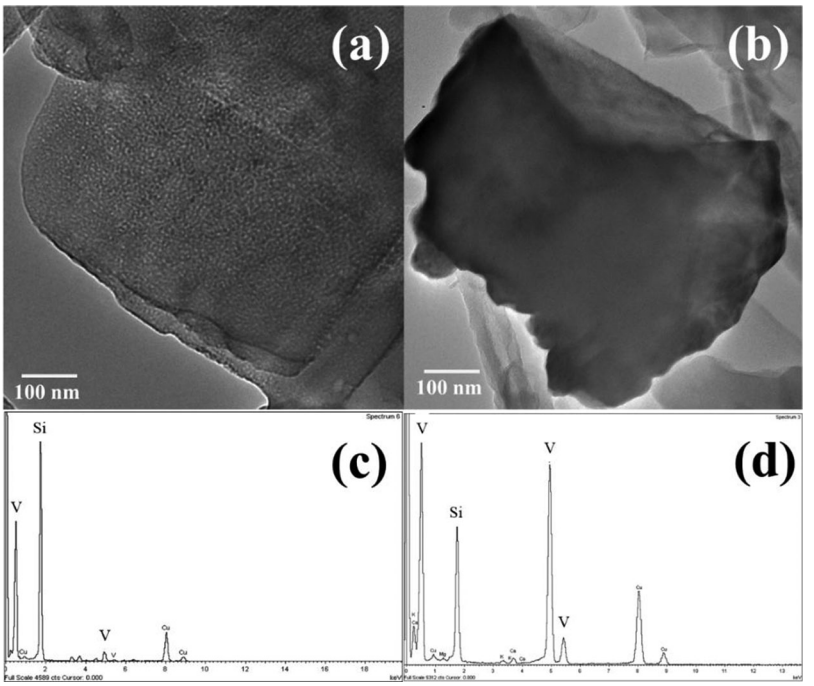

Figure 8. TEM and EDX images of (a) and (c) 6 hr-400W, (b) and (d) 6 hr-600W.

sintering. This synthesis method is very simple, rapid, safe, free solvent and easy to work on. Such a synthesis process is a challenging for the synthesis of vanadium silicate compounds, as previously it was done by closed-system method. The heating at 600 W provided the highest specific capacitance was 376 F g^{-1} at 5 m V^{-1} of scan rate. The impurity phase at 600 W as Li_2SiO_3 could enhance the specific capacitance of the product. The specific capacitance of the product indicated its performance could be used as an electrode material. The results of XRD, SEM, and TEM-EDX are the reasons to explain the specific capacitance of synthesized $Li_{3.6}Si_{0.6}V_{0.4}O_4$ by solid-state reaction with microwave-assisted method.

Acknowledgments

The authors would like to thank National Research Council of Thailand (NRCT) for the financial support and Synchrotron Light Research Institute (Public Organization) (BL5.2), Nakhon Ratchasima, Thailand.

References

1. Y. Wang et al., A review for the synthesis methods of lithium vanadium phosphate cathode materials, *J. Mater. Sci.* **28**, 18269 (2017).
2. J. K. Helen et al., Modern microwave methods in solid-state inorganic materials chemistry: From fundamentals to manufacturing, *Chem. Rev.* **114**, 1170 (2014).
3. L. Huiqiao et al., Li_3VO_4: A promising insertion anode material for lithium-ion batteries, *Adv. Energy Mater.* **3** (4), 428 (2013). DOI: 10.1002/aenm.201200833.

4. S. Bhawan, and S. A. Kumar et al., Synthesis of hierarchical mesoporous vanadium silicate-1 zeolite catalysts for styrene epoxidation with organic hydroperoxide, *J. Mater. Chem. A* **2**, 1930 (2014).
5. L. Grzegorz et al., Carbon nanotubes and their composites in electrochemical applications, *Energy Environ. Sci.* **4**, 1592 (2011).
6. X. Mingquan et al., Li^+-conductive Li_2SiO_3 stabilized Li-rich layered oxide with an in situ formed spinel nano-coating layer: Toward enhanced electrochemical performance for lithium-ion batteries, *RSC Adv.* **6** (41), 34245 (2016). DOI: 10.1039/C6RA00769D.
7. R. R. Mishra, and A. K. Sharma, A review of research trends in microwave processing of metal-based materials and opportunities in microwave metal casting, *Crit. Rev. Solid State* **41** (3), 217 (2016). DOI: 10.1080/10408436.2016.1142421.
8. Q. Rong et al., Layered cobalt nickel silicate hollow spheres as a highly-stable supercapacitor material, *Appl. Energy* **153**, 63 (2015). DOI: 10.1016/j.apenergy.2014.11.077.
9. N. A. Khan, and S. H. Jhung, Synthesis of metal-organic frameworks (MOFs) with microwave or ultrasound: Rapid reaction, phase-selectivity, and size reduction, *Coord. Chem. Rev.* **285**, 11 (2015). DOI: 10.1016/j.ccr.2014.10.008.
10. S. Weiwei, L. Hao, and W. Yong, Microwave-assisted synthesis of graphene nanocomposites: Recent developments on lithium-ion batteries, *Rep. Electrochem.* **5**, 1 (2015). DOI: 10.2147/RIE.S65118.
11. G. T. Zhou et al., Microwave-assisted synthesis of graphene nanocomposites: Recent developments on lithium-ion batteries, *J. Mater. Chem.* **13** (10), 2607 (2003). DOI: 10.1039/b303163b.
12. G. Yang et al., Microwave solid-state synthesis and electrochemical properties of carbon-free $Li_3V_2(PO_4)_3$ as cathode materials for lithium batteries, *Electrochim. Acta* **55** (8), 2951 (2010). DOI: 10.1016/j.electacta.2009.11.102.
13. Z. Chen et al., High-performance supercapacitors based on hierarchically porous graphite particles, *Adv. Energy Mater.* **1** (4), 551 (2011). DOI: 10.1002/aenm.201100114.
14. T.-Y. Wei et al., A cost-effective supercapacitor material of ultrahigh specific capacitances: Spinel nickel cobaltite aerogels from an epoxide-driven sol-gel process, *Adv. Mater.* **22** (3), 347 (2010). DOI: 10.1002/adma.200902175.
15. G. Huang et al., Fabrication of vanadium oxide with different valences embedded carbon 7fibers and their electrochemical performance for supercapacitor, *New J. Chem.* 1 (2017).
16. J. Yan et al., Rapid microwave-assisted synthesis of graphene nanosheet/Co_3O_4 composite for supercapacitors, *Electrochim. Acta* **55** (23), 6973 (2010). DOI: 10.1016/j.electacta.2010.06.081.
17. D. Xiao et al., Hydrothermal preparation of iron-based orthosilicate cathode materials with different SiO_2 particles and their electrochemical properties, *Int. J. Electrochem. Sci.* **8**, 7581 (2013).
18. M. Vijayakumar et al., Vibrational and impedance spectroscopic studies on lithium vanadate prepared by solid-state reaction, *Mater. Lett.* **57** (22–23), 3618 (2003). DOI: 10.1016/S0167-577X(03)00137-X.
19. H. Kruger, V. Kahlenberg, and R. Kaindl, $Li_2Si_3O_7$: Crystal structure and Raman spectroscopy, *J. Solid State Chem.* **180** (3), 922 (2007). DOI: 10.1016/j.jssc.2006.12.015.
20. M. K. Trivedi et al., Spectroscopic characterization of disodium hydrogen orthophosphate and sodium nitrate after biofield treatment, *J. Chromatogr. Sep. Tech.* **6**, 1 (2015).
21. O. N. Koroleva, The structure of lithium silicate melts revealed by high-temperature Raman spectroscopy, *Spectrosc. Lett.* **50** (5), 257 (2017). DOI: 10.1080/00387010.2017.1316743.
22. G. Hu et al., Effects of Li_2SiO_3 coating on the performance of $LiNi_{0.5}Co_{0.2}Mn_{0.3}O_2$ cathode material for lithium ion batteries, *J. Alloys Compd.* **690**, 589 (2017). DOI: 10.1016/j.jallcom.2016.08.187.
23. Q. Wang et al., Synthesis of graphene supported Li_2SiO_3/Li_2SnO_3 anode material for rechargeable lithium ion batteries, *Appl. Surf. Sci.* **469**, 253 (2019). DOI: 10.1016/j.apsusc.2018.11.055.

24. L. Shen et al., Carbon-coated Li_3VO_4 spheres as constituents of an advanced anode material for high-rate long-life lithium-ion batteries, *Adv. Mater.* **1701571**, 1 (2017).
25. J. Jiang et al., Investigation of the reversible intercalation/deintercalation of Al into the novel Li_3VO_4@C microsphere composite cathode material for aluminum-ion batteries, *ACS Appl. Mater. Interfaces* **9** (34), 28486− (2017). DOI: 10.1021/acsami.7b07503.
26. K. Toda et al., Synthesis of nano-sized materials using novel water assisted solid state reaction method, *Key Eng. Mater.* **777**, 163 (2018). DOI: 10.4028/www.scientific.net/KEM.777.163.
27. N. Laorodphan et al., Effect of B_2O_3 content on structure-function of vanadium-lithium-borate glasses probed by synchrotron-based XAS and vibrating sample magnetrometry technique, *J. Non-Cryst. Solids* **497**, 56 (2018). DOI: 10.1016/j.jnoncrysol.2018.04.045.
28. A. Montreeuppathum et al., Effect of borate glass network to electrochemical properties: Manganese doped lithium borate glasses, *Radiat. Phys. Chem.* **170**, 108677 (2020). DOI: 10.1016/j.radphyschem.2019.108677.
29. K. I. Rybakov et al., Microwave heating of conductive powder materials, *J. Appl. Phys.* **99**, 1 (2006).
30. T. Bok et al., Effective strategies for improving the electrochemical properties of highly porous Si foam anodes in lithium-ion batteries, *J. Mater. Chem.* **2** (34), 14195 (2014). DOI: 10.1039/C4TA02392G.
31. B. D. D. Grenu et al., Recent progress of microwave-assisted synthesis of silica materials, *J. Nanomater.* **10**, 1 (2020).
32. E. Janiszewska et al., One-pot synthesis of vanadium-containing silica SBA-3 materials and their catalytic activity for propene oxidation, *RSC Adv.* **9** (9), 4671 (2019). DOI: 10.1039/C8RA10171J.
33. S. S. Gundale, and A. V. Deshpande, Improvement of ionic conductivity in $L_{i3.6}Si_{0.6}V_{0.4}O_4$ ceramic inorganic electrolyte by addition of $LiBO_2$ glass for Li ion battery application, *Electrochim. Acta* **265**, 65 (2018). DOI: 10.1016/j.electacta.2018.01.122.
34. S. Caes et al., Mesoporous lithium vanadium oxide as a thin film electrode for lithium-ion batteries: Comparison between direct synthesis of LiV_2O_5 and electrochemical lithium intercalation in V_2O_5, *J. Mater. Chem. A* **2** (16), 5809 (2014). DOI: 10.1039/C4TA00090K.